NANO LETTERS

Letter

pubs.acs.org/NanoLett

Plasmon–Plasmon Hybridization and Bandwidth Enhancement in Nanostructured Graphene

Damon B. Farmer,*[,†] Daniel Rodrigo,[‡,§] Tony Low,[∥] and Phaedon Avouris[†]

[†]IBM T. J. Watson Research Center, Yorktown Heights, New York 10598, United States

[‡]Institute of Electrical Engineering and [§]Institute of Bioengineering, École Polytechnique Fédérale de Lausanne (EPFL), Lausanne 1015, Switzerland

[∥]Department of Electrical & Computer Engineering, University of Minnesota, Minneapolis, Minnesota 55455, United States

ABSTRACT: Graphene plasmonic structures with long-range layering periodicity are presented. Resonance energy scaling with the number of graphene layers involved in plasmonic excitation allows these structures to support multiple plasmonic modes that couple and hybridize due to their physical proximity. Hybridized states exhibit bandwidth enhancements of 100–200% compared to unhybridized modes, and resonance energies deviate from what is usually observed in coupled plasmonic systems. Origins of this behavior are discussed, and experimental observations are computationally modeled. This work is a precursor and template for the study of plasmonic hybridization in other two-dimensional material systems with layering periodicity.

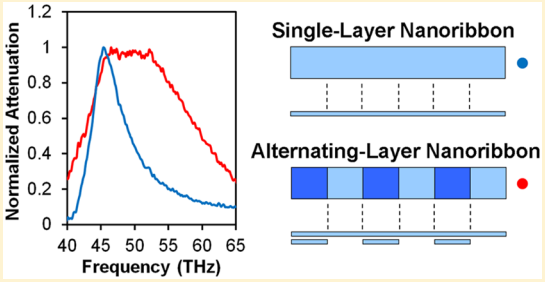

KEYWORDS: *Graphene, plasmon, hybridization, infrared, bandwidth, spectroscopy*

Graphene plasmonics is a relatively new research area that offers the potential of photonic device applications in the mid- and far-infrared regions of the electromagnetic spectrum.[1,2] Resonance energy tunability, subwavelength confinement, and relatively long plasmon lifetime are some of the properties that make graphene an interesting plasmonic material.[3,4] Indeed, graphene plasmons have already shown utility in surface sensing[5] and photodetection[6] applications and as terahertz polarizers and notch filters.[7] Within these applications, it is desirable to have the ability to manipulate the light absorption behavior of the plasmons. The resonance frequency associated with a plasmonic mode can be tuned by modifying the carrier density in graphene,[3] the electrostatic environment around graphene,[5] or the physical dimensions of the graphene structure,[8] while the resonance intensity can be increased by stacking graphene layers.[7] While demonstrations of tuning these properties exist, there has been no investigation of systematically tuning the absorption width. Bandwidth enhancement is particularly relevant in surface sensing and optical filtering, where a broader band allows for an increased operation range. Here, we present a method to manipulate this property by plasmon–plasmon hybridization. The graphene structure used to accomplish this is designed to support different resonance modes in adjacent regions of the material, where communication between the modes results in the formation of a hybrid resonance state with a bandwidth enhancement of approximately 100–200%.

Plasmon excitation is achieved through charge confinement attained in graphene nanoribbons, where plasmons with energies in the mid-infrared are produced. The basic configuration of the plasmonic structure being investigated is shown in Figure 1a. Here, nanoribbons are fabricated with alternating, periodic regions of one and two graphene layers. These alternating layer (AL) nanoribbons are grouped in parallel arrays to form the measurement structures, where incident light polarized perpendicular to the nanoribbon length can excite plasmons due to the width confinement.[3] The arrays are fabricated by first patterning conventional nanoribbon arrays in a single layer of graphene (Figure 1b, steps 1–3). A second layer of graphene is then transferred onto the first layer,[9] and nanoribbon patterning is repeated with the mask pattern rotated 90° (Figure 1b, steps 4–6), resulting in formation of the AL nanoribbon structure. Within this process, the graphene layers are exposed to nitric acid vapor for 5 min at 25 °C to increase their doping.[10] Also, to facilitate Fourier transform infrared (FTIR) transmission spectroscopy, the arrays are fabricated on high resistivity substrates (280 nm SiO_2/Si) with an overall array size of at least 60 μm × 60 μm, larger than the diameter of the FTIR beam (25 μm). The nanoribbon widths as well as the lengths of the AL segments are designed to be 100 nm after etching, with spacing between adjacent nanoribbons also 100 nm. Example images of conventional nanoribbon arrays and AL nanoribbon arrays are shown in Figure 1c and d, where the layered patterning is evident in the AL case. Raman spectroscopy of the AL arrays reveals prominent defect related peaks, indicative of the large concentration of graphene nanoribbon edges in the structure (Figure 1e).[11,12] Furthermore, relative shifts of the G and 2D

Received: January 13, 2015
Revised: February 27, 2015
Published: March 6, 2015

DOI: 10.1021/acs.nanolett.5b00148
Nano Lett. 2015, 15, 2582–2587

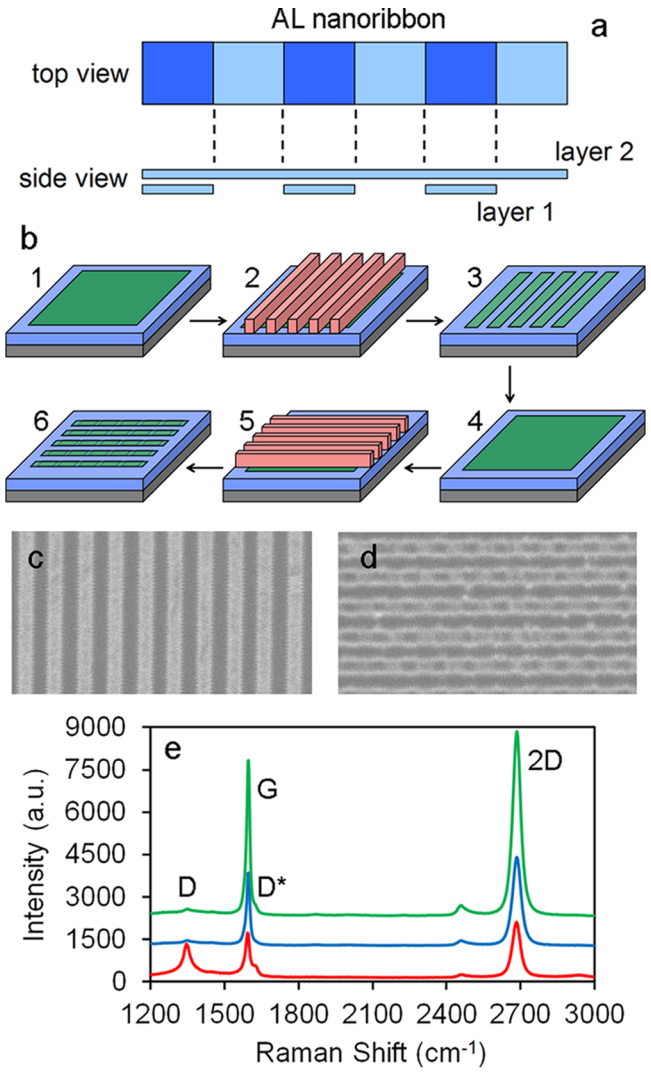

Figure 1. (a) Illustration of the basic graphene structure shows how the segmented layer 1 underneath the continuous layer 2 forms a nanoribbon in which the number of layers alternates along the ribbon length. (b) Schematic diagram of the sample fabrication procedure illustrates the six basic steps involved in making arrays of this structure: (1) first graphene transfer, (2) mask deposition and patterning, (3) graphene etching and mask removal, (4) second graphene transfer, (5) mask deposition and 90° patterning, and (6) graphene etching and mask removal. Poly(methyl methacrylate) (PMMA) is used as the etch mask, which is patterned using electron-beam lithography and removed in acetone at 25 °C. Oxygen plasma is used as the graphene etchant. (c,d) SEM micrographs show the differences between a conventional nanoribbon array (c) and an AL array (d). Their orientations are rotated to match their respective schematic orientations in (b) 3 and 6. The nanoribbon widths and lengths of the alternating layered segments are approximately 100 nm. (e) Raman spectroscopy of the AL array (red) reveals significant defect related peaks, D and D*, as compared to spectra of single-layer (blue) and double-layer graphene (green).

peaks indicate that there is no significant difference between the doping levels of the bulk and nanoribbon regions.[13] A Fermi energy (E_F) of 317 meV is determined from the position of the G peak, which corresponds to an approximate carrier concentration of (7−8) × 10^{12} cm^{-2}.[14]

The two regions of the AL nanoribbon independently exhibit different plasmon resonance energies because the resonance frequency increases as more graphene layers are added. This is shown by comparing the resonances of one, two, and three stacked layers in Figure 2a. The blueshift with increasing layer

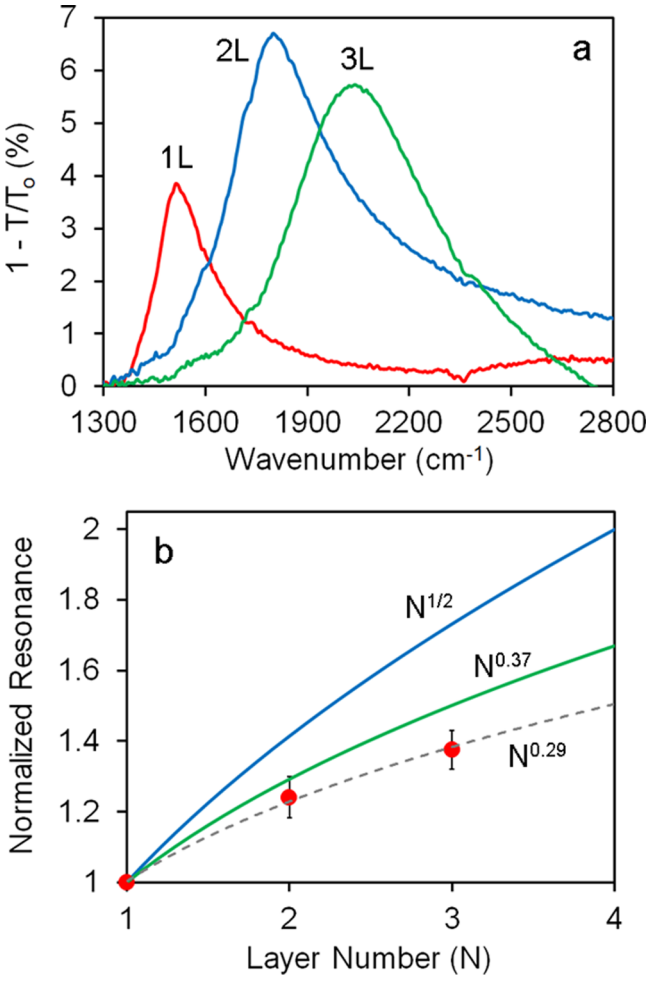

Figure 2. (a) Extinction spectra in the mid-infrared of one-, two-, and three-layer conventional (i.e., continuous, not AL) graphene nanoribbon arrays shows how the plasmon resonance increases with the number of layers. (b) This increase is observed to be sublinear, with $\omega \propto N^{\alpha}$, where an experimental value of $\alpha = 0.29$ is obtained (dots with fitted dashed line). Values of $\alpha = 1/2$ and $\alpha = 0.37$ are computed assuming a nondispersive and dispersive SiO_2 substrate, respectively, with $d = 0$. In the nondispersive case, a high-frequency dielectric constant of 2 is used (refractive index 1.42) over the entire frequency range.

number (N) can be understood as a hybridization caused by the different possible plasmon dipole orientations among the graphene layers in the stack, a phenomenon that is commonly observed in stacked metamaterials.[15] This has been previously observed in graphene plasmonic layered structures, where the layers are separated by polymer spacers and the plasmon frequency (ω) scales as $N^{1/2}$.[7] This scaling can be understood in terms of the optical conductivity (σ) in graphene. When intraband electronic processes dominate, this conductivity follows the Drude model, where $\sigma \propto E_F \propto n^{1/2}$ and n is the carrier concentration. With N layers, this becomes $N\sigma \propto NE_F \propto Nn^{1/2}$, and since ω is proportional to the square root of E_F, the scaling relation $\omega \propto N^{1/2}n^{1/4}$ is attained.[2]

In the present study, the resonance is observed to scale as $N^{0.29}$ (Figure 2b). Deviation from $N^{1/2}$ could arise primarily for two reasons. First, the plasmons interact with optical phonons

DOI: 10.1021/acs.nanolett.5b00148
Nano Lett. 2015, 15, 2582−2587

in the SiO_2 substrate,[16] which increases the energy of the plasmon resonance.[8] The strength of this plasmon−phonon coupling decreases with increasing N, thus altering the scaling behavior. This can be modeled computationally using finite element methodology (FEM),[17] where the ideal $N^{1/2}$ behavior is reproduced when allowing for static screening without phonon dispersion, and a $N^{0.37}$ behavior is observed after introducing phonon interactions (Figure 2b). Further deviation of the scaling can develop in the presence of a finite interlayer distance (d) that allows for decay of the plasmon field between the layers and subsequent diminishing of the interlayer coupling. The general scaling in this case is $\omega \propto N^{\alpha}$, where $0 < \alpha < 1/2$, with $\alpha = 1/2$ corresponding to $d = 0$ in the absence of phonon interactions and $\alpha = 0$ corresponding to $d \rightarrow \infty$. The measured value $\alpha = 0.29$ suggests that even though the layers are consecutively stacked with no intentional spacer, $d \neq 0$. This may be because the transfer and patterning processes of graphene can both induce wrinkles and result in residue contamination (e.g., from undissolved resist) on the graphene surface, making $d > 0$.[18−20] As aforementioned, a previous study of graphene plasmons in graphene/polymer stacks reported ideal $N^{1/2}$ scaling.[7] Reasons that this system did not exhibit the behavior observed presently are 2-fold. First, interactions with the SiO_2 phonon are suppressed in all but the bottom graphene layer because of the relatively thick polymer spacers used between layers (~20 nm), providing appreciable separation from the SiO_2 surface. Second, that study dealt with plasmon resonances in the far-infrared wavelengths as opposed to the mid-infrared wavelengths studied here. These longer wavelengths allow for comparatively better coupling between graphene layers, as the out-of-plane plasmon field penetration depth scales with the incident wavelength, effectively reducing the effect of a finite d.

The plasmonic absorption behavior exhibited by the AL nanoribbon structure deviates from the absorption behavior of the conventional nanoribbons discussed above. Figure 3a shows the plasmonic absorption characteristics of this structure as it progresses through the fabrication process illustrated in Figure 1b. Once the first layer of graphene is deposited, and the first nanoribbon array is fabricated, an expected single plasmon resonance peak is observed. Transferring the second graphene layer onto the array damps this plasmon oscillation, causing the absorption to essentially vanish. A new resonance peak then appears upon the second patterning and completion of the AL array. Resonance from a double-layer array of identical nanoribbon width is also shown in Figure 3a for comparison. It is clear that the AL resonance does not correspond to the single-layer or double-layer case, its energy is rather somewhere in between. Furthermore, the width of the AL resonance peak is greater than the other resonance peaks. The single-layer and double-layer peaks have half widths of 190 cm^{-1} (5.7 THz) and 310 cm^{-1} (9.3 THz), respectively, while the half width of the AL peak is 620 cm^{-1} (18.6 THz). Peak width is generally expected to increase with plasmon energy, as the number of damping channels increases.[8] The AL nanoribbon absorption represents deviation from this monotonic behavior. It is also noted that the decrease in magnitude of the AL absorption peak as compared to the single-layer and double-layer peaks is not a result of damping-induced broadening but is rather due to a relative reduction of the filling factor of the constituent single-layer and double-layer nanoribbon regions in the AL array.

Consistency and reproducibility of these plasmonic absorption characteristics are illustrated in Figure 3b, where two

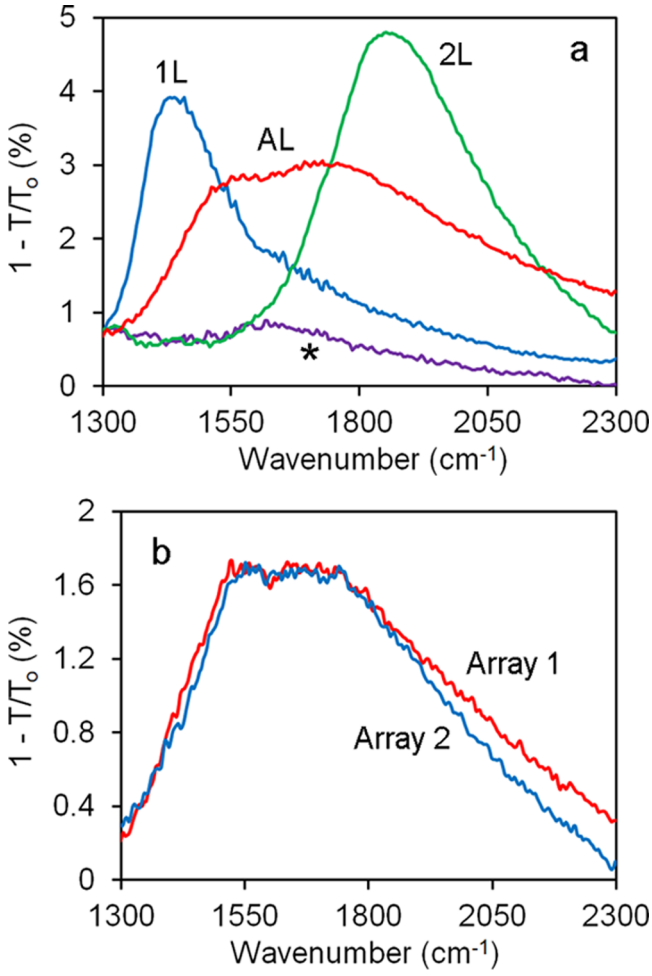

Figure 3. (a) Extinction spectra comparing the plasmon resonance of graphene nanoribbon arrays composed of one layer (1L), two layers (2L), and the alternating layer structure (AL). Plasmon excitation is damped when the continuous second graphene layer is placed on top of the nanoribbon array of the first layer (*). (b) Spectra of two different arrays shows the reproducibility of the plateau-like peaks produced by the AL structure. The two line shapes are macroscopically similar, with attenuation rates of 0.0065%/cm^{-1} (0.0024%/cm^{-1}) for Array 1 and 0.0067%/cm^{-1} (0.0030%/cm^{-1}) for Array 2 on the low (high) energy side of the maximum absorption.

separate AL nanoribbon array structures with identical geometries are compared. The two line shapes exhibit similar attenuation rates on both the low energy and high energy sides of the maximum absorption. The asymmetric nature of these line shapes, with a higher attenuation rate on the low energy side, is indicative of Fano resonance that is ubiquitous in graphene plasmonic systems.[2] It is the flat, plateau-like, maximum absorption that is unique. The width of this region is approximately 260 cm^{-1} (7.8 THz) for both arrays. This region of the line shape is distinctly different from typical resonance behavior in that it cannot be modeled by a single Fano fit.

In order to better understand this line shape effect, AL nanoribbon arrays are fabricated with a single layer of hexagonal boron nitride (BN) inserted between the two graphene layers. This is accomplished by incorporating a BN transfer step after patterning of the first nanoribbon array, before transfer of the second graphene layer (between step 3 and step 4 in Figure 1b). The BN serves as a spacer material, reducing the

DOI: 10.1021/acs.nanolett.5b00148
Nano Lett. 2015, 15, 2582−2587

electrostatic coupling strength between the layers by increasing *d*. Doing this results in a narrowing of the peak width from 240 cm^{-1} (7.2 THz) to 130 cm^{-1} (3.9 THz) (Figure 4a). This

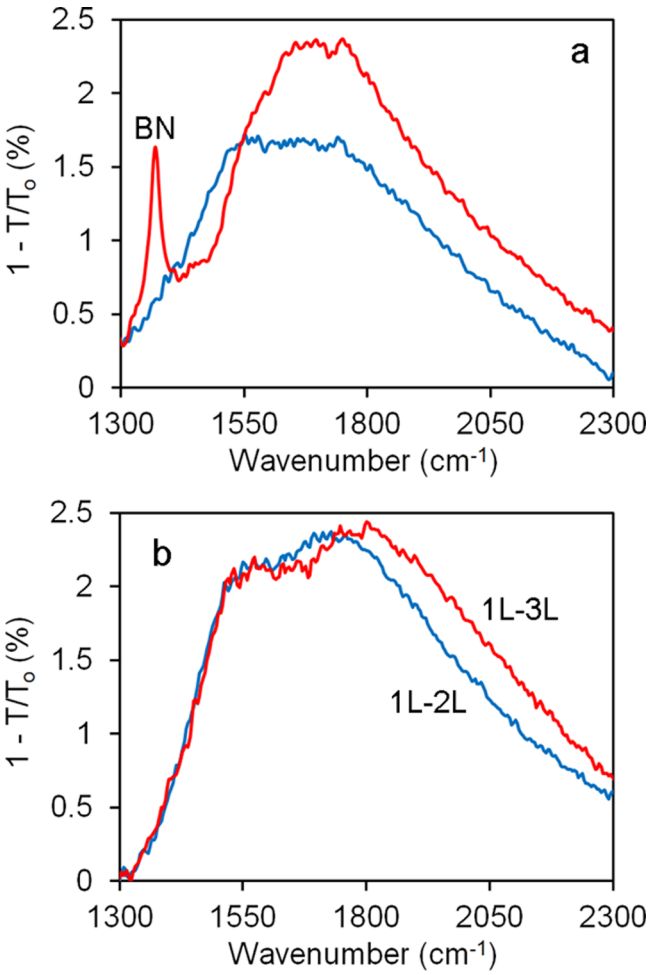

Figure 4. (a) Comparison of AL structures with (red) and without (blue) a BN layer inserted between the two graphene layers. The BN absorption peak is clearly visible in the former configuration. Spacing provided by the BN results in a narrowing of the resonance peak width. (b) Comparison of AL structures with one-layer and two-layer regions (1L−2L) and one-layer and three-layer regions (1L−3L). The latter configuration results in a wider peak width.

demonstrates that the origin of the plateau lies in the ability to excite two distinct plasmon modes that can electrostatically couple. As *d* increases, the double-layer regions develop more of the single-layer resonance character, and the absorption peak becomes sharper as a result. This is consistent with the scaling behavior aforementioned, where the plasmon resonance no longer scales significantly with *N* as *d* increases.

Resonance peak width can also be increased by increasing the energy difference of the plasmons supported by the constituent regions of the AL structure. This is shown in Figure 4b, which compares the absorption spectra of a single/double layer AL nanoribbon array to the spectra of a single/triple layer AL nanoribbon array. The single/triple layer structure is fabricated by incorporating a third graphene transfer step before the second etching (step 4 in Figure 1b). The additional layer results in a 17% increase of the half width, from 580 cm^{-1} (17.4 THz) to 680 cm^{-1} (20.4 THz). The ability to both increase and decrease the widths of these line shapes illustrates a level of control over the absorption properties of the system. However, the rate of width increase is limited by the sublinear scaling behavior shown in Figure 2b.

Plasmonic response of complex nanostructures is typically explained as an analogy of orbital hybridization, where coupling between localized plasmons leads to energy splitting and the formation of symmetric and antisymmetric coupled states.[21] However, a straightforward application of this methodology to the experimental system presented above proves to be insufficient. Coupled nanostructures that support different intrinsic plasmon modes are anticipated to produce hybridized modes that are higher and lower in energy than their intrinsic modes,[22,23] an expectation that is contrary to the observed AL nanoribbon behavior. It is suggested that this discrepancy originates from the fact that the top graphene layer of the AL nanoribbon (layer 2 in Figure 1a) is electrically continuous, thus prohibiting the treatment of the single-layer and double-layer segments as individual monomers, as is done in orbital theory. A different analysis must therefore be performed in order to describe the plasmonic behavior of the AL structure.

The charge distributions and corresponding electric moments of the extrema energy configurations of single-layer, double-layer, and AL nanoribbons are schematically illustrated in Figure 5a. While one configuration is possible in the single-layer nanoribbon, the moments in the two layers of the double-layer nanoribbon can align either parallel or antiparallel, with the latter being inactive to incident light due to cancellation of their dipole moments. The plasmon frequency of the double-layer nanoribbon is greater than the single-layer nanoribbon of the same width and carrier concentration because the additional charge offered by the second layer increases the energy of the parallel configuration, which can be deduced by comparing path A in Figure 5a. The constituent regions of the AL nanoribbon also possess these qualities, but electrostatic coupling between the two regions causes the energetics to differ. For the single-layer and double-layer nanoribbons, charge on one side is symmetrically attracted to opposite charge on the other side. In the AL structure, breaking this symmetry at the layer interface, path B in Figure 5a, causes the energetics to deviate. The charge in the single-layer region is now more strongly attracted due to the additional charge across the interface in the double-layer region, and vice versa. This results in blueshifting of the single-layer plasmon and redshifting of the double-layer plasmon and qualitatively explains both the observed position of the hybridized resonance being between the two constituent resonances and the broad line shape of the resonance, a result of the coupled resonance peaks merging.

Beyond this phenomenological picture, the basic experimental observations can also be described computationally with electrodynamic Maxwell simulations. Here, FEM is applied to a three-dimensional unit cell with single-layer and double-layer periodicity, which is defined by two pairs of perfect magnetic and electric boundary conditions on the surfaces delimiting the cell. The graphene is modeled as a two-dimensional surface enforcing an impedance boundary condition, where the ratio between electric and magnetic field phasors is equal to the graphene Drude conductivity,[17] and finer meshing is enforced over the graphene surface to capture the subwavelength nature of the plasmonic mode. Simulation results are shown in Figure 5b, where, as in the experiments, the hybrid resonance is found to be positioned between the intrinsic resonances of the single-layer and double-layer nanoribbons. Furthermore, the relatively broad line shape of

DOI: 10.1021/acs.nanolett.5b00148
Nano Lett. 2015, 15, 2582−2587

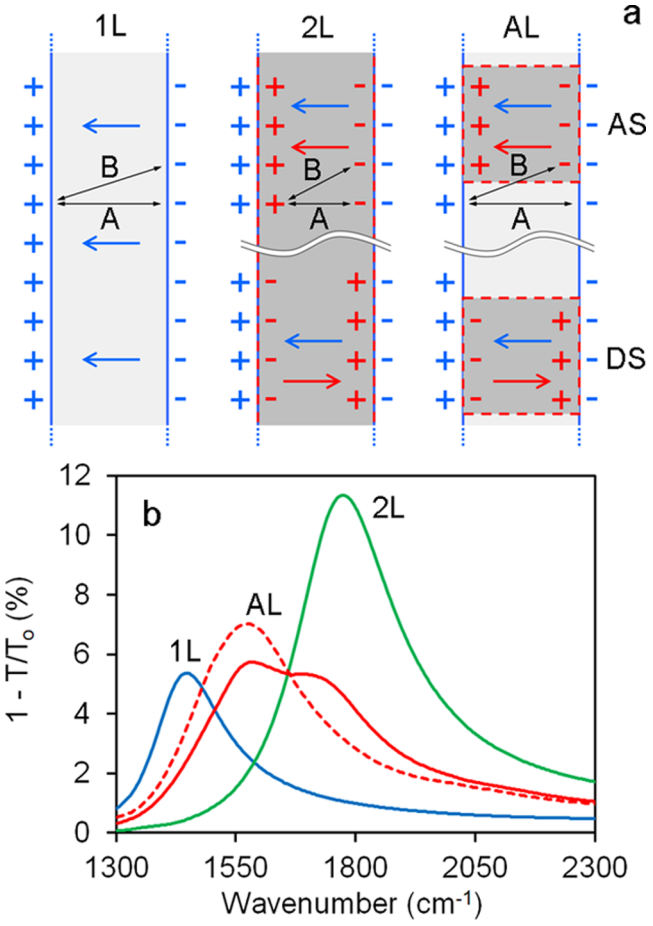

Figure 5. (a) Schematics of the charge distribution and corresponding electric moments of single-layer, double-layer, and AL nanoribbons. Comparing the relative energetics along path A and B allows for a phenomenological understanding of the experimental observations. The dark state (DS) and active state (AS) light absorption configurations for double-layer and AL nanoribbons are denoted. (b) Computational simulations of plasmon absorption behavior for single-layer, double-layer, and AL nanoribbons. The simulation parameters used for these examples include 72 nm for the nanoribbon widths, 100 nm for the AL segment lengths, interlayer spacings of 10 nm (AL and 2L, solid lines) and 20 nm (dashed line), an interlayer dielectric constant of $\kappa = 1$, and a carrier concentration of 1.6×10^{13} cm^{-2}.

the resonance peak is reproduced and is observed to narrow as the interlayer spacing is increased, in agreement with the experimental observations presented in Figure 4a. Differences in the magnitude of plasmon absorption between the experimental and simulated results originates from damping processes in the physical system that are not taken into account in the simulations.[8] Material and dimensional parameters must also be approximated since the simulations do not factor in this and other nonidealities present in the experiment. Nevertheless, the fact that the qualitative absorption behavior of this structure can be simulated opens the possibility of exploring and predicting the behavior of AL nanoribbons with different dimensions, and even other structures with more complex layered configurations.

The ability to modify plasmon activity by layering gives graphene a degree of freedom that is not as easily accessible in conventional materials. This property is complemented by the ease with which graphene features can be patterned, allowing for top-down fabrication of complex layered nanostructures with long-range order. Here, these properties are exploited to facilitate an unconventional hybridization of plasmon modes and realize subsequent broadening of the absorption band. As with metamaterials, the AL nanoribbon array discussed above is only one of many possible layered, multiresonance nanostructures that is feasible, and not just with graphene. As the library of two-dimensional materials continues to grow, it will be interesting to explore how their combinations can be utilized using similar layering and patterning techniques to make other novel multiresonance and hybridized resonance plasmonic structures.

AUTHOR INFORMATION

Corresponding Author

*E-mail: dfarmer@us.ibm.com.

Notes

The authors declare no competing financial interest.

ACKNOWLEDGMENTS

The authors are grateful to J. Bucchignano and S. Dawes for expert technical assistance involving electron-beam lithography. Single-layer graphene on Cu foil was obtained from Bluestone Global Tech, and single-layer hexagonal BN on Cu foil was obtained from Graphene Supermarket.

REFERENCES

(1) Grigorenko, A. N.; Polini, M.; Novoselov, K. S. *Nat. Photonics* **2012**, *6*, 749−758.
(2) Low, T.; Avouris, P. *ACS Nano* **2014**, *8*, 1086−1101.
(3) Ju, L.; Geng, B.; Horng, J.; Girit, C.; Martin, M.; Hao, Z.; Bechtel, H. A.; Liang, X.; Zettl, A.; Ron Shen, Y.; Wang, F. *Nat. Nanotechnol.* **2011**, *6*, 630−634.
(4) Yan, H.; Li, Z.; Li, X.; Zhu, W.; Avouris, P.; Xia, F. *Nano Lett.* **2012**, *12*, 3766−3771.
(5) Li, Y.; Yan, H.; Farmer, D. B.; Meng, X.; Zhu, W.; Osgood, R. M.; Heinz, T. F.; Avouris, P. *Nano Lett.* **2014**, *14*, 1573−1577.
(6) Freitag, M.; Low, T.; Zhu, W.; Yan, H.; Xia, F.; Avouris, P. *Nat. Commun.* **2013**, *4*, 4:1951.
(7) Yan, H.; Li, X.; Chandra, B.; Tulevski, G.; Wu, Y.; Freitag, M.; Zhu, W.; Avouris, P.; Xia, F. *Nat. Nanotechnol.* **2012**, *4*, 330−334.
(8) Yan, H.; Low, T.; Zhu, W.; Wu, Y.; Freitag, M.; Li, X.; Guinea, F.; Avouris, P.; Xia, F. *Nat. Photonics* **2013**, *7*, 394−399.
(9) Li, X.; Cai, W.; An, J.; Kim, S.; Nah, J.; Yang, D.; Piner, R.; Velamakanni, A.; Jung, I.; Tutuc, E.; Banerjee, S. K.; Colombo, L.; Ruoff, R. S. *Science* **2009**, *324*, 1312−1314.
(10) Bae, S.; Kim, H.; Lee, Y.; Xu, X.; Park, J.-S.; Zheng, Y.; Balakrishnan, J.; Lei, T.; Kim, H. R.; Song, Y. I.; Kim, Y.-J.; Kim, K. S.; Ozyilmaz, B.; Ahn, J.-H.; Hong, B. H.; Iijima, S. *Nat. Nanotechnol.* **2010**, *5*, 574−578.
(11) Casiraghi, C.; Hartschuh, A.; Qian, H.; Piscanec, S.; Georgi, C.; Fasoli, A.; Novoselov, K. S.; Basko, D. M.; Ferrari, A. C. *Nano Lett.* **2009**, *9*, 1433−1441.
(12) Ryu, S.; Maultzsch, J.; Han, M. Y.; Kim, P.; Brus, L. E. *ACS Nano* **2011**, *5*, 4123−4130.
(13) Das, A.; Pisana, S.; Chakraborty, B.; Piscanec, S.; Saha, S. K.; Waghmare, U. V.; Novoselov, K. S.; Krishnamurthy, H. R.; Geim, A. K.; Ferrari, A. C.; Sood, A. K. *Nat. Nanotechnol.* **2008**, *3*, 210−215.
(14) Yan, H.; Xia, F.; Zhu, W.; Freitag, M.; Dimitrakopoulos, C.; Bol, A. A.; Tulevski, G.; Avouris, P. *ACS Nano* **2011**, *5*, 9854−9860.
(15) Liu, N.; Guo, H.; Fu, L.; Kaiser, S.; Schweizer, H.; Giessen, H. *Nat. Mater.* **2008**, *7*, 31−37.
(16) Kitamura, R.; Pilon, L.; Jonasz, M. *Appl. Opt.* **2007**, *46*, 8118−8133.
(17) Tamagnone, M.; Gómez-Díaz, J. S.; Mosig, J. R.; Perruisseau-Carrier, J. *J. Appl. Phys.* **2012**, *101*, 214102.

DOI: 10.1021/acs.nanolett.5b00148
Nano Lett. 2015, 15, 2582−2587

(18) Chae, S. J.; Gunes, F.; Kim, K. K.; Kim, E. S.; Han, G. H.; Kim, S. M.; Shin, H.-J.; Yoon, S.-M.; Choi, J.-Y.; Park, M. H.; Yang, C. W.; Pribat, D.; Lee, Y. H. *Adv. Mater.* **2009**, *21*, 2328−2333.
(19) Liang, X.; Sperling, B. A.; Calizo, I.; Cheng, G.; Hacker, C. A.; Zhang, Q.; Obeng, Y.; Yan, K.; Peng, H.; Li, Q.; Zhu, X.; Yuan, H.; Hight Walker, A. R.; Liu, Z.; Peng, L.; Richter, C. A. *ACS Nano* **2011**, *5*, 9144−9153.
(20) Zhu, W.; Low, T.; Perebeinos, V.; Bol, A. A.; Zhu, Y.; Yan, H.; Tersoff, J.; Avouris, P. *Nano Lett.* **2010**, *12*, 3431−3436.
(21) Prodan, E.; Radloff, C.; Halas, N. J.; Nordlander, P. *Science* **2003**, *302*, 419−422.
(22) Sheikholeslami, S.; Jun, Y.; Jain, P. K.; Alivisatos, A. P. *Nano Lett.* **2010**, *10*, 2655−2660.
(23) Jain, P. K.; Eustis, S.; El-Sayed, M. A. *J. Phys. Chem. B* **2006**, *110*, 18243−18253.

DOI: 10.1021/acs.nanolett.5b00148
Nano Lett. 2015, 15, 2582−2587